Model-based mechanical and control design of a three-axis platform

J.M. Rodriguez-Fortun [a,*], J. Orus [a], J. Alfonso [a], J.R. Sierra [a], F. Buil [a], F. Rotella [b], J.A. Castellanos [c]

[a] Grupo de Investigación Aplicada (GIA-MDPI), Instituto Tecnológico de Aragón, Zaragoza, Spain
[b] ENIT, Tarbes, France
[c] Instituto de Ingeniería de Aragón, Universidad de Zaragoza, Spain

A B S T R A C T

Keywords:
Positioning
Tracking
Modeling
Differential flatness
Control
Hysteresis

In recent times, the interest from scientific and industrial community for the micrometric range has observed an important growth. The advances in microelectronics or the research on microbiology are just two examples of fields requiring technologies capable of assuring accurate displacements in that range. The present work focuses on the mechanical and control design of a micrometer range positioning and tracking platform using mathematical models. In a first phase, these models permit to identify the relationship between the dynamic performance of the structure and the mechanical properties of the elements that compose it. At the very beginning of the design, this information is used for the development of the different parts of the platform. Afterwards, once an initial design is finished and 3D models are available, the design is refined using finite element tools. In parallel to the mechanical design, the knowledge of the system embodied in the mathematical model is profited in the design of a control strategy for tracking and positioning. The proposed control strategy combines a linear controller based on differential flatness with a hysteresis compensator for correcting this nonlinear effect of the piezoelectric actuators. In the present paper, the mathematical derivation of the system model, its application to the design and validation of the platform and the final closed loop experimental evaluation are described.

1. Introduction

This paper is focused on the design of a micrometer range positioning and tracking platform with 3 degrees of freedom for metrological applications. This type of platforms has gained interest in the last years because of the new requirements appeared in different fields of industry, such as microelectronics or nanostructured coatings, and of the scientific research, such as microbiology, medicine or material science, just to name a few. The design methodology described in the present paper shows the importance of simplified mathematical models for both the mechanical and control design of this sort of platforms. These models permit the designer to identify the correspondence between the different components of the device and its final performance in a quantitative way, while at the same time are fundamental for the development of control strategies for obtaining the smoothest and most accurate response.

The kinematics of the designed platform follows the structure described in [13]. This structure is based on a tripod and it uses a combination of links and joints that improves its stiffness and compactness. With respect to [13], the elements used in the present paper have been adapted to the specific requirements and actuator type of our application. Apart from this structure, the list of designs in the bibliography is enormous and different approaches can be found depending on the final application. Just considering the number of degrees of freedom, we can find devices with 1 degrees of freedom [11,12], with 2 degrees of freedom [15], with 3 degrees of freedom [10,14], with 6 degrees of freedom [4,16] or other combinations depending on specific applications.

Most of the examples mentioned above use flexure hinges as joints between elements. These joints are based on deformable elements which have a much lower stiffness in some degrees of freedom with respect to the others. They assure low friction movements, reduce backlash effects and have a linear behavior in small displacements. Therefore, they are used in positioning systems and other mechanical devices, like microgrippers [18]. The design formulation of these elements can be found in recent papers, like [22,23], or in reference books [19 21]. The design and sizing of these elements must take into account both the stiffness of the joint in the direction of interest, and in the other degrees of freedom. For this reason, we present a methodology for defining the stiffness of the flexures taking into consideration its effect on the final performance of the platform using simplified static and dynamic models.

The movement of the platform is obtained using piezoelectric actuators. These devices are characterized by extremely high accuracy and resolution in very short strokes. Their limited stroke is overcome in the present project by using mechanical amplification. Although piezoelectric actuators are extensively used in micrometer range positioning devices, it is possible to find other approaches, like DC linear motors [5], electrostatic actuators [6] or Shape Memory Alloys [17].

As it happens with the kinematics of the positioning platforms, the design of the control is mainly affected by the final application and the characteristics of the device. In consequence, different approaches can be found in the literature, like classical PID, backstepping [7], robust compliant control [8], differential flatness [9], among others. A point to have into consideration is the hysteresis present in piezoelectric actuators and which should be compensated for minimizing dynamic tracking errors in large stroke actuations. Typical examples of compensation techniques are inverse models [25], neural controller [26], fuzzy controller [27] or high gain feedback controllers with notch filters for avoiding instabilities [30]. In [31], the behavior variability in different regions caused by the hysteresis phenomenon is compensated using robust H_∞ design strategies. In repetitive applications, iterative control is also used [29]. The present work combines a feedforward feedback strategy designed using differential flatness [1 3], with a hysteresis compensator [28]. The former permits decoupling the 3 degrees of freedom of the platform and simplifies the design procedure by using an equivalent trivial representation of the system dependent only on the trajectory to follow. The latter linearizes the system behavior by compensating the capacitance variation in the actuator caused by the hysteresis. For this compensation, despite inverting previously identified models, an on line sensor based estimator is used.

The description of the platform under analysis is presented in Section 2. The mathematical model of the system appears in Section 3. This model is furtherly used in Section 4 for the design of the control strategy. The experimental validation of the model and the control strategy are the contents of Section 5. Finally, Section 6 contains the conclusions of the work. A summary of the nomenclature is included in the Appendix A. Two more Appendices B and C have been included for defining the coefficients obtained during the derivation of the different models.

2. Three axis platform

Fig. 1(left) shows the designed platform. It is based on a tripod with three actuation lines shifted 120°. It has three main degrees of freedom: x and y axis rotation (θ_x, θ_y), and elevation in a direction perpendicular to the xy plane (z). A detail of one actuation line and its elements appears in Fig. 1(right). Qualitatively, one actuation

line is composed of a horizontal beam between links $P1$ and $P2$, a lever with a link $P3$ and a vertical pillar between joints $P4$ and $P5$. Fig. 1 also shows the unions $Pp1$ and $Pp2$, where the piezoelectric actuator is placed. The actuator is responsible for generating a horizontal displacement ($\delta_{1,i}$ in Fig. 1(right)), which is afterwards transformed into a vertical movement x_i in the pillar of the actuation line i using the lever (a, b or c in Fig. 1(left)). Taking into consideration the restriction of movement between the three actuation lines once the upper platform is mounted, it can be assumed that the direction of movement x_i of the actuation line is perfectly vertical. This design presents an increased stiffness in torsional and horizontal displacements of the platform with respect to the typical tripod because of the restricted degrees of freedom in the flexures. In this connection, the flexures are normally designed to work just in one direction. Only the flexures that link the upper platform have 2 degrees of freedom for allowing the rotation of the platform. Apart from that, the horizontal placement of the actuator reduces the overall thickness of the device.

The piezoelectric actuators are APA 120ML from Cedrat Group. These actuators use a cymbal structure for mechanically amplifying its movement, and are characterized by a great robustness to tangential misalignments. This last point is of great interest taking into account the tolerances in the manufacture of the different parts of the platform.

For closing the control loop, the platform has the following sensors:

- Three accelerometers on the upper platform at the positions a, b and c (Fig. 1). The complete device with the accelerometers used for the experimental validation appears in Section 5.
- Strain sensors embedded in the piezoelectric actuators.

3. Mathematical model of the three axis platform

The design methodology described in this paper is based on the generation of a mathematical description of the platform. In this section this representation is derived in two consecutive steps:

- Mechanical level: a purely mechanical representation for relating the stiffness of the different flexures with the global stiffness of the platform. This representation will be afterwards used as reference for sizing the flexures and it is a very important help for the mechanical engineer. As any free mechanical body, the upper platform has 6 degrees of freedom: three of them, from now on principal degrees of freedom, correspond to the controlled movements of the platform (z, θ_x, θ_y) and the remaining ones, from now on restricted degrees of freedom, correspond to the uncontrolled movements (x, y, θ_z).
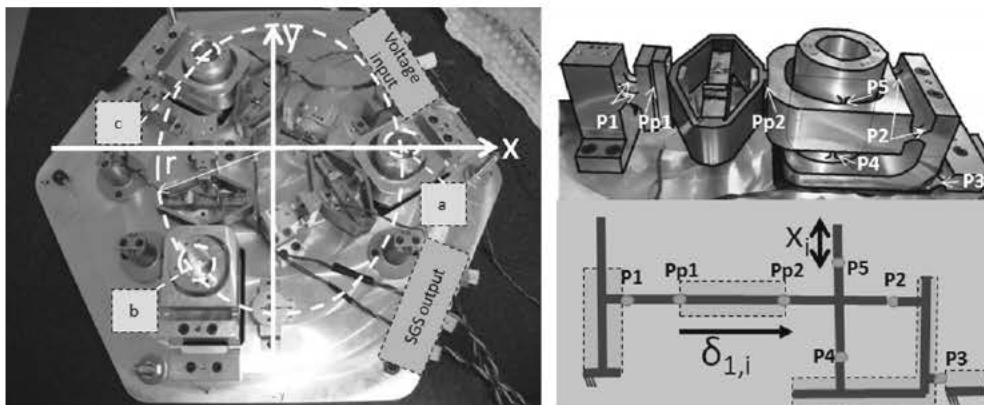

Fig. 1. Design of the system: (left) general view without the upper platform and (right) detail of one actuation line.

- Electromechanical level: the mechanical model is coupled with the electrical command system by describing the actuator behavior. This representation will be used for the design of the control strategy.

3.1. Dynamic mechanical model in the principal degress of freedom

The displacement of the platform is a consequence of the vertical movement of the three actuation lines previously described (Fig. 2). Therefore, the representation of the latters is the first step for obtaining the complete dynamic mechanical model.

The complete coordinates of one actuation line i are defined by the deformation values for the hinges and the bars (Figs. 1 and 3): displacement (x_i), deformation of the flexures ($\alpha_{1,i}, \alpha_{2,i}, \alpha_{3,i}, \alpha_{4,i}, \alpha_{5,i}$), deformation of the beam ($\delta_{1,i}$) and deformation of the pillar ($\delta_{3,i}$). However, all these variables are not independent and can be geometrically coupled:

- The displacement x_i (Fig. 3) is a result of the deformation in the system:

$$x_i \quad \delta_{3,i} + \frac{b}{a}\delta_{1,i} \qquad (1)$$

- Assuming small displacements, the angles in the different joints can be approached as:

$$\begin{aligned}
\alpha_{1,i} &\approx \frac{\delta_{1,i}\tan\beta}{L_1} \approx 0 \\
\alpha_{2,i} &\quad \alpha_{1,i} + \alpha_{3,i} \\
\alpha_{3,i} &\approx \frac{\delta_{1,i}}{t_4\cos\beta} \approx \frac{\delta_{1,i}}{a} \\
\alpha_{4,i} &\approx \alpha_{3,i} + \alpha_{5,i} \approx \alpha_{3,i} \\
\alpha_{5,i} &\approx \frac{\alpha_{3,i}t_5}{L_3} \approx 0
\end{aligned} \qquad (2)$$

where the geometrical parameters β, t_4, L_1 and L_3 are defined in Figs. 2 and 3.

Consequently, the kinematics of an actuation line just requires two generalized coordinates: $\delta_{1,i}$ and $\delta_{3,i}$. The rest of the variables can be expressed as function of these two.

From the point of view of the force and torque equilibrium at the lever, the force externally applied F_i and the force in the horizontal beam $F_{1,i}$ can be related as:

$$F_{1,i} \quad \frac{1}{a}\left(F_i b + k_{b,1}\alpha_1 + k_{b,2}\alpha_{2,i} + k_{b,3}\alpha_{3,i} + k_{b,4}\alpha_{4,i} + k_{b,5}\alpha_{5,i}\right) \qquad (3)$$

where it is clearly observed that the force exerted by the piezoelectric actuator $F_{1,i}$ has to move the external load F_i and the elastic
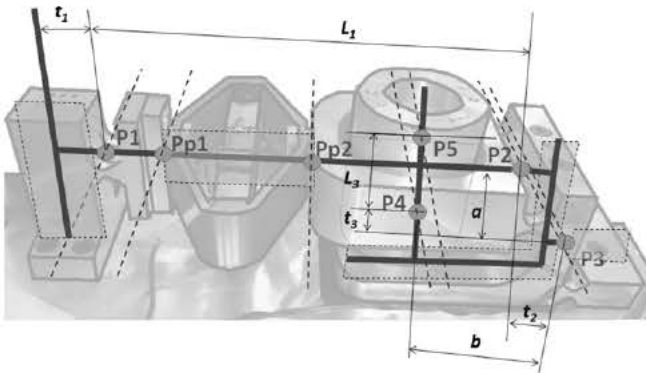

Fig. 2. Main elements and dimensions of one actuation line. The figure shows also the principal rotation axis of the flexures -dashed line-.

deformation from the hinges. In this connection, the application of an external force F_i on the actuation line i causes a displacement x_i and increases the elastic energy stored in the line:

$$\begin{aligned}
F_i x_i \quad &\frac{1}{2}k_{e1}(\delta_{1,i} \quad \delta_{p,i})^2 + \frac{1}{2}k_{e3}\delta_{3,i}^2 + \frac{1}{2}k_{b,1}\alpha_{1,i}^2 + \frac{1}{2}k_{b,2}\alpha_{2,i}^2 \\
&+ \frac{1}{2}k_{b,3}\alpha_{3,i}^2 + \frac{1}{2}k_{b,4}\alpha_{4,i}^2 + \frac{1}{2}k_{b,5}\alpha_{5,i}^2
\end{aligned} \qquad (4)$$

where k_{e1} and k_{e3} are the equivalent axial stiffness of beam and pillar, $k_{b,j}$ is the bending stiffness of the flexure j in the turning direction of Fig. 3 and $\delta_{p,i}$ is the displacement caused by the piezoelectric actuator.

Considering (1) and (2) and (4) can be expressed as:

$$\begin{aligned}
F\left(\delta_{3,i} + \frac{b}{a}\delta_{1,i}\right) \quad &\frac{1}{2}k_{e1}(\delta_{1,i} \quad \delta_{p,i})^2 + \frac{1}{2}k_{e3}\delta_{3,i}^2 \\
&+ \frac{1}{2}(k_{b,2} + k_{b,3} + k_{b,4})\frac{\delta_{1,i}^2}{a^2}
\end{aligned} \qquad (5)$$

Given the energy state in (5), the effect of a small variation in $\delta_{3,i}$ results in:

$$\delta_{3,i} \quad \frac{F_i}{k_{e3}} \qquad (6)$$

which relates the deformation of the pillar $\delta_{3,i}$ with the applied force F_i.

A small variation of $\delta_{1,i}$ in (5), shows the relationship between the applied force F_i and the deformation of the beam $\delta_{1,i}$, which is related with the rotation of the different flexures:

$$\frac{b}{a}F_i \quad k_{e1}(\delta_{1,i} \quad \delta_{p,i}) + (k_{b,2} + k_{b,3} + k_{b,4})\frac{\delta_{1,i}}{a^2} \qquad (7)$$

(7) can be expressed in terms of (3):

$$\delta_{1,i} \quad \delta_{p,i} \quad \frac{F_{1,i}}{k_{e1}} \qquad (8)$$

This expression shows the deformation of the beam is a combination of the deformation of the actuator $\delta_{p,i}$ and its elastic compression because of the force $F_{1,i}$.

Using (1), (8), (6) and (3), one actuation line can be represented as an elastic element and a force actuator working in parallel:

$$F_i \quad A_2^{-1}A_1\delta_{p,i} \quad A_2^{-1}x_i \qquad (9)$$

where A_1 and A_2 can be found in Appendix B.

Now it is easy to obtain the complete mechanical model, which is expressed in terms of its global coordinates $\mathbf{x} = (z, \theta_x, \theta_y)^T$. These last can be expressed in terms of the displacement of the three actuation lines $\mathbf{x}_{abc} = (x_a, x_b, x_c)^T$ as:

$$\mathbf{x} \quad \left(\mathbf{T}_f^T\right)^{-1}\mathbf{x}_{abc} \qquad (10)$$

$\mathbf{T}_f \in R_{3\times3}$ is the geometrical transformation between the two bases (Appendix A).

The force exerted by the three actuation lines $\mathbf{f}_{abc} = (F_a, F_b, F_c)^T$ can also be expressed as global forces (F) and torques (Γ) on the platform $\mathbf{f} = (F_z, \Gamma_x, \Gamma_y)^T$ assuming a conservative power conversion:

$$\mathbf{f} \quad \mathbf{T}_f\mathbf{f}_{abc} \qquad (11)$$

The dynamic equation is obtained by using the Lagrangian function L expressed in the global coordinates and forces:

$$L \quad T \quad U \qquad (12)$$

In this expression, T is the kinetic energy:

$$T \quad \frac{1}{2}\dot{\mathbf{x}}^T\mathbf{M}\dot{\mathbf{x}} \qquad (13)$$

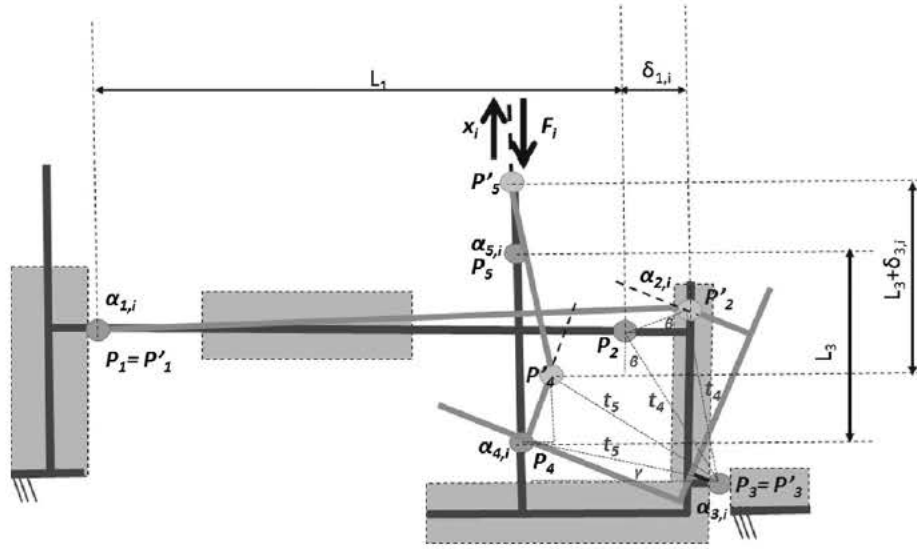where $\mathbf{M} \in R_{3\times3}$ is the inertia matrix.

Fig. 3. Angles of actuation line i when the piezoelectric actuator changes its length.

U is the potential energy stored because of the deformation of the actuation lines (9) and the stiffness of the links between the actuation lines and the upper platform ($\mathbf{D} \in R_{3\times3}$):

$$U = \frac{1}{2}\mathbf{x}^T\left(\mathbf{T}_f\mathbf{A}_2{}^1\mathbf{T}_f^T\right)\mathbf{x} + \frac{1}{2}\mathbf{x}^T\mathbf{D}\mathbf{x} \tag{14}$$

The derivation of the Lagrangian results in:

$$\frac{\partial}{\partial t}\frac{\partial L}{\partial \dot{\mathbf{x}}} - \frac{\partial L}{\partial \mathbf{x}} = \mathbf{C}_v\dot{\mathbf{x}} + \mathbf{T}_f\mathbf{A}_2{}^1\mathbf{A}_1\Delta_{abc} = \mathbf{f}_{ext} \tag{15}$$

where the terms on the right are the non conservative forces: $\mathbf{C}_v \in R_{3\times3}$ is the viscous friction associated with the actuation lines, $\mathbf{A}_2{}^1\mathbf{A}_1 \in R_{3\times3}$ is the effect of the piezoelectric actuator (9) expressed in vector form with $\Delta_{abc} = (\delta_{p,a}, \delta_{p,b}, \delta_{p,c})$, and $\mathbf{f}_{ext} \in R_{3\times1}$ are the forces and torques externally applied on the platform.

This expression can be written in a more intuitive way as:

$$\ddot{\mathbf{x}} = -\mathbf{M}^{-1}\mathbf{C}_v\dot{\mathbf{x}} - \mathbf{M}^{-1}\left(\mathbf{T}_f\mathbf{A}_2{}^1\mathbf{T}_f^T + \mathbf{D}\right)\mathbf{x} + \mathbf{M}^{-1}\mathbf{T}_f\mathbf{A}_2{}^1\mathbf{A}_1\Delta_{abc}$$
$$+ \mathbf{M}^{-1}\mathbf{f}_{ext} \tag{16}$$

Using (16), the state space representation of the mechanical system is:

$$\begin{pmatrix} \dot{\mathbf{x}} \\ \ddot{\mathbf{x}} \end{pmatrix} = \mathbf{A}_m\begin{pmatrix} \mathbf{x} \\ \dot{\mathbf{x}} \end{pmatrix} + \mathbf{B}_m\begin{pmatrix} \Delta_{abc} \\ \mathbf{f}_{ext} \end{pmatrix} \tag{17}$$

where $\mathbf{A}_m \in R_{6\times6}$ and $\mathbf{B}_m \in R_{6\times6}$.

(17) is used for estimating the mechanical resonance frequencies of the platform in the permitted degrees of freedom.

Two expressions must be derived because of its importance for calculating the hysteresis compensator:

- Using (3) and (8) the force in the actuator i ($F_{1,i}$) can be obtained as:

$$F_{1,i} = B_1F_i + B_2x_i \tag{18}$$

- Using (9), (10) and (16), it is possible to obtain the value of $\mathbf{f}$:

$$\mathbf{f} = \mathbf{M}\ddot{\mathbf{x}} + \mathbf{C}_v\dot{\mathbf{x}} + \mathbf{D}\mathbf{x} + \mathbf{f}_{ext} \tag{19}$$

3.2. Static mechanical model in the restricted degress of freedom

Taking into consideration the relative position of the three actuation lines (Fig. 1) and the stiffness of every actuation line in the
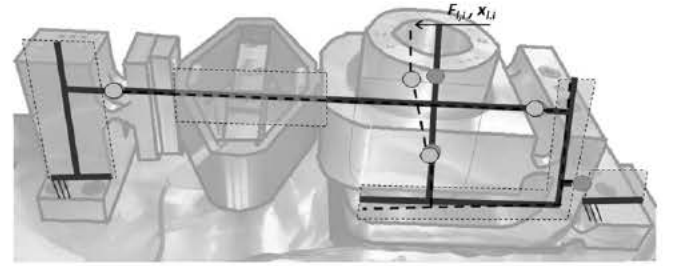

Fig. 4. Displacement of actuation line i when pushed in its longitudinal direction of movement.
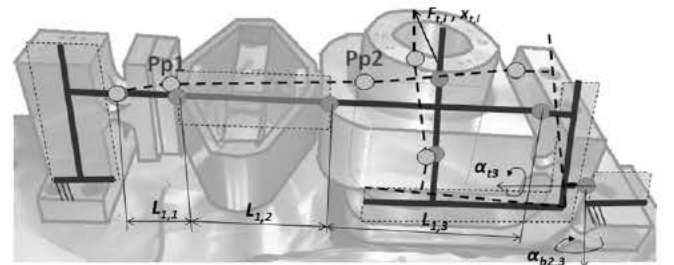

Fig. 5. Displacement of actuation line i when pushed in its transversal direction of movement.

longitudinal k_l^{al} (Fig. 4) and transversal direction k_t^{al} (Fig. 5), the stiffness of the platform in the restricted degrees of freedom (displacement $x \to k_x$, displacement $y \to k_y$, torsion k_{bz}) can be estimated as:

$$k_x \approx k_l^{al}(2\cos(\pi/6)) + k_t^{al}(1 + 2\sin(\pi/6))$$
$$k_y \approx k_l^{al}(1 + 2\sin(\pi/6)) + k_t^{al}(2\cos(\pi/6)) \tag{20}$$
$$k_{bz} \approx k_l^{al}(3\sin(\pi/6)) + k_t^{al}(3\cos(\pi/6))$$

where k_l^{al} and k_t^{al} is the stiffness of a single actuation line in the longitudinal (Fig. 4) and the transversal direction (Fig. 5).

Using a similar procedure to that used for obtaining the formula (9), the expressions for k_l^{al} and k_t^{al} are obtained:
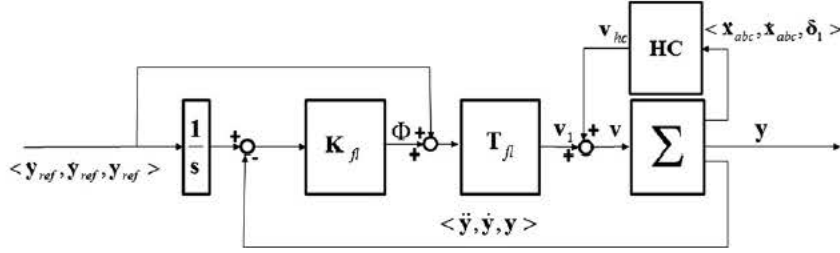
Fig. 6. Diagram of the control strategy showing: $\mathbf{K}_{fl}$, the closed loop compensator in the flat coordinates; $\mathbf{T}_{fl}$, transformation between the flat states and the output voltage; and **HC** is the hysteresis compensator.

- The stiffness in the longitudinal direction of movement $\left(k_l^{al}\right)$ assumes the following kinematical constraints between the different coordinates (similarly as done with (2)):

$$\alpha_{1,i} \approx 0$$
$$\alpha_{2,i} \approx \alpha_{3,i} \approx \frac{F_{1,i}}{k_{e1}a}$$
$$\alpha_{5,i} \approx \frac{x_{l,i}}{L_3}$$

(21)

where $x_{l,i}$ is the longitudinal displacement of the actuation line (Fig. 4). In this case, the force applied in the structure causes the turning of the pillar and, as a consequence of this effect, the torque appearing in the lever is balanced by a slight force in the beam and a rotation in the lever. The obtained equivalent stiffness calculated as $F_{l,i}/x_{l,i}$ is:

$$k_l^{al} \approx \frac{k_{b,4}k_{b,5} + (k_{b,4}+k_{b,5})(k_{b,2}+k_{b,3}+a^2 k_{e1})}{k_{b,4}(L_3 - aa) + L_3(k_{b,2}+k_{b,3}+k_{e1}a^2)} \frac{1}{L_3}$$

(22)

where $\bar{a} \approx L_2 - a$ (Fig. 2).

- The same procedure is used for obtaining k_t^{al}. In this case, the deformation of the system is more complex than before because the force applied results in both a torsion ($\alpha_{t,3}$) and a rotation ($\alpha_{b2,3}$) of the lever (Fig. 5). The geometrical assumptions are:

$$\alpha_{b2,5,i} \approx \frac{x_{t,i} - \alpha_{b2,3,i}b}{L_3}$$
$$\alpha_{b2,5,i} \approx \alpha_{b2,4,j} + \alpha_{t3}$$
$$\alpha_{t3,i} \approx \alpha_{t1,i} + \alpha_{t2,i} + \alpha_{tp1,i} + \alpha_{tp2,i}$$
$$\alpha_{t3,i}a \approx \alpha_{b2,1,i}L_{1,1} + (\alpha_{b2,1,i}+\alpha_{b2,p1,i})L_{1,2} + (\alpha_{b2,1,i}+\alpha_{b2,p1,i}+\alpha_{b2,p2,i})L_{1,3}$$
$$\alpha_{b2,3,i} \approx \alpha_{t4,i} + \alpha_{t5,i}$$
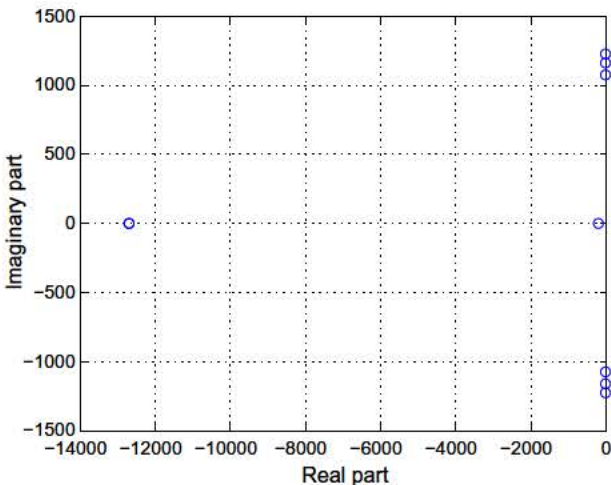$$\alpha_{b2,2,i} \approx \alpha_{b2,1,i} + \alpha_{b2,p1,i} + \alpha_{b2,p2,i} + \alpha_{b2,3,i}$$

(23)

Fig. 7. Roots of the error dynamics (35).

Table 1
Roots of the error dynamics.

−12,694	−12,696	−12,698	−9 ± 1227i	−8 ± 1162i
−7 ± 1075i	−200	−200	−200	–

where $\alpha_{tj,i}$ is the torsion of flexure j in the actuation line i and $\alpha_{b2,j,i}$ is the rotation of flexure j in the actuation line i in a rotation axis perpendicular to the torsion one and to the principal one in Fig. 2 (see Fig. 5). The stiffness related with these angles are $k_{t,j}$ and $k_{b2,j}$. The obtained expression for $F_{t,i}/x_{t,i}$ is:

$$k_t^{al} \approx \frac{(k_{b2,5}+k_{b2,4}G_4)G_7 + k_{b2,4}G_5}{L_3} \frac{1}{(k_{b2,5}+k_{b2,4}G_4)G_8 - k_{b2,4}G_6}$$

(24)

where the values G_i appear in Appendix C.

3.3. Electromechanical model of the platform

The representation (17) is extended to take into account the electromechanical coupling caused by the piezoelectric actuator. From an electrical point of view, the actuator is represented with a capacitor C, whose value changes due to hysteresis, a resistance R_e from the actuator to the amplifier, and a voltage source dependent on the mechanical load $F_{1,i}$ (direct piezoelectric effect) [24]:

$$V_i \approx R_e \dot{q}_i + \frac{q_i}{C'} - a_{pzt}F_{1,i}$$

(25)

with V_i the voltage applied to the actuator, q_i the charge in the capacitor C and a_{pzt} the transformation factor of the piezoelectric actuator.

Due to the indirect piezoelectric effect, the displacement of the actuator $\delta_{p,i}$ is proportional to the charge:

$$\delta_{p,i} \approx a_{pzt}q_i$$

(26)

Now, the system representation can be done using the voltage input in the three actuation lines **v**, and including the charge in the three capacitors as a new state of the system $\mathbf{q} = (q_a, q_b, q_c)^T$. The obtained system using a mean value C in place of C' is:

$$\begin{pmatrix}\dot{\mathbf{x}}\\ \ddot{\mathbf{x}}\\ \dot{\mathbf{q}}\end{pmatrix} \approx \begin{pmatrix}\mathbf{0}_{3\times3} & \mathbf{1}_{3\times3} & \mathbf{0}_{3\times3}\\ \mathbf{H}_1 & \mathbf{H}_2 & \mathbf{H}_3\\ \mathbf{H}_4 & \mathbf{H}_5 & \mathbf{H}_6\end{pmatrix}\begin{pmatrix}\mathbf{x}\\ \dot{\mathbf{x}}\\ \mathbf{q}\end{pmatrix} + \begin{pmatrix}\mathbf{0}_{3\times3}\\ \mathbf{0}_{3\times3}\\ \mathbf{H}_7\end{pmatrix}\mathbf{v}_1 \equiv \mathbf{A}_{ss}\mathbf{x}_{ss} + \mathbf{B}_{ss}\mathbf{v}_1$$

(27)

with $\mathbf{A}_{ss} \in R_{9\times9}$, $\mathbf{B}_{ss} \in R_{9\times3}$, $\mathbf{x}_{ss} \in R_{9\times1}$ and $\mathbf{v}_1 \in R_{3\times1}$. The Appendix B shows the detail of the terms in the model.

Due to the low value of $\mathbf{f}_{ext}$ in the application, this term has been neglected in (27).

System (27), which is controllable, and the compensation of C are the basis of the control strategy.
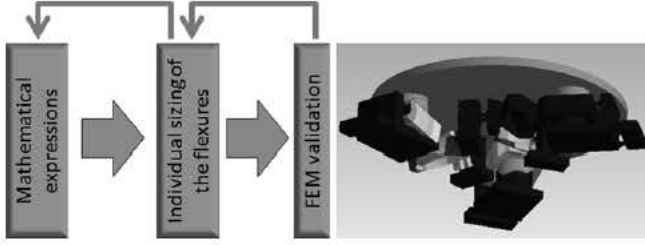
Fig. 8. Flow chart describing the sizing procedure based on the theoretical expressions obtained in Section 3.

4. Model-based control of the system

In this section the control strategy implemented in the system is described. This strategy takes advantage of the model presented in previous section and shows the highly simplification that results in the design of the controller. The control design presented in this section is based on the differential flatness in (27) [9] and on a hysteresis compensator that linearizes the behavior of the actuators by compensating the variations in the capacitor value C' (Fig. 6).

4.1. Differential flatness

Differential flatness is a property of a system which permits to express its states $\mathbf{x} \in R_{n\times1}$ and inputs $\mathbf{u} \in R_{m\times1}$ in terms of the so called *flat outputs* $\mathbf{y} \in R_{m\times1}$ and a finite number of their derivatives [1 3].

For linear systems, every controllable linear system is flat [3]. In the case of (27), the position vector $\mathbf{x}$ is the flat output $\mathbf{y} \in R_{3\times1}$ and the equivalence between the original and the flat representation can be expressed by means of the following diffeomorphism:

- In one direction:

$$
\begin{aligned}
\mathbf{x} &\quad \mathbf{y} \\
\dot{\mathbf{x}} &\quad \dot{\mathbf{y}} \\
\mathbf{q} &\quad \mathbf{H}_3^{-1}(\quad \ddot{\mathbf{y}} \quad \mathbf{H}_1\mathbf{y} \quad \mathbf{H}_2\dot{\mathbf{y}})
\end{aligned}
\tag{28}
$$

- In the other direction:

$$
\begin{aligned}
\mathbf{y} &\quad \mathbf{x} \\
\dot{\mathbf{y}} &\quad \dot{\mathbf{x}} \\
\ddot{\mathbf{y}} &\quad \mathbf{H}_1\mathbf{x} \quad \mathbf{H}_2\dot{\mathbf{x}} \quad \mathbf{H}_3\mathbf{q}
\end{aligned}
\tag{29}
$$

The input control can also be described in terms of the *flat outputs*:

$$
\begin{aligned}
\mathbf{v}_1 \quad T_{fl}(\Phi,\ddot{\mathbf{y}},\dot{\mathbf{y}},\mathbf{y}) &\quad \mathbf{H}_7^{-1}\mathbf{H}_3^{-1}\Phi + \left(\mathbf{H}_7^{-1}\mathbf{H}_3^{-1}\mathbf{H}_2 + \mathbf{H}_7^{-1}\mathbf{H}_6\mathbf{H}_3^{-1} \right)\ddot{\mathbf{y}} \\
&+ \left(\mathbf{H}_7^{-1}\mathbf{H}_3^{-1}\mathbf{H}_1 \quad \mathbf{H}_7^{-1}\mathbf{H}_5 + \mathbf{H}_7^{-1}\mathbf{H}_6\mathbf{H}_3^{-1}\mathbf{H}_2 \right)\dot{\mathbf{y}} \\
&+ \left(\mathbf{H}_7^{-1}\mathbf{H}_4 + \mathbf{H}_7^{-1}\mathbf{H}_6\mathbf{H}_3^{-1}\mathbf{H}_1 \right)\mathbf{y} \\
\mathbf{K}_{m1}\Phi &+ \mathbf{K}_{m2}\ddot{\mathbf{y}} + \mathbf{K}_{m3}\dot{\mathbf{y}} + \mathbf{K}_{m4}\mathbf{y}
\end{aligned}
\tag{30}
$$

with $\mathbf{K}_{mi} \in R_{3\times3}$ for $i = 1, 2, 3, 4$. Using (28) and (30), the system (27) transformed into the new variables has the trivial shape:

$$
\dddot{\mathbf{y}} \quad \Phi
\tag{31}
$$

with $\Phi \in R_{3,1}$ the input of the system.

4.2. Control strategy

Fig. 6 shows the control strategy implemented in the positioning platform. It is based on two elements:

- Flatness based control: the control command in terms of voltage is:

$$
\mathbf{v}_1 \quad \mathbf{v}_{1,ff} + \mathbf{v}_{1,fb}
\tag{32}
$$

where $\mathbf{v}_{1,ff}$ is the theoretical command for following the trajectory $\mathbf{y}_{ref}$ calculated with (30), and $\mathbf{v}_{1,fb}$ is a compensator feedback term ($\mathbf{v}_{1,fb}$) for attenuating the effect of perturbations:

$$
\begin{aligned}
\mathbf{v}_{1,ff} &\quad \mathbf{K}_{m1}\dddot{\mathbf{y}}_{ref} + \mathbf{K}_{m2}\ddot{\mathbf{y}}_{ref} + \mathbf{K}_{m3}\dot{\mathbf{y}}_{ref} + \mathbf{K}_{m4}\mathbf{y}_{ref} \\
\mathbf{v}_{1,fb} &\quad \mathbf{K}_{m1}\mathbf{K}_{fl}\ddot{\mathbf{e}} + \mathbf{K}_{m2}\mathbf{K}_{fl}\dot{\mathbf{e}} + \mathbf{K}_{m3}\mathbf{K}_{fl}\mathbf{e} + \mathbf{K}_{m4}\mathbf{K}_{fl} \int \mathbf{e}\,dt
\end{aligned}
\tag{33}
$$

In the expressions above, $\mathbf{e} = \mathbf{y}_{ref}$ $\mathbf{y}$, and K_{mi} are obtained from (30) for $i = 1, 2, 3, 4$.

Using (30), $\mathbf{v}_1$ can be expressed in terms of the flat input as:

$$
\begin{aligned}
\Phi &\quad \dddot{\mathbf{y}}_{ref} + \mathbf{K}_{fl}\ddot{\mathbf{e}} + \mathbf{K}_{m1}^{-1}(\mathbf{K}_{m2}\mathbf{K}_{fl}\dot{\mathbf{e}} + \mathbf{K}_{m3}\mathbf{K}_{fl}\mathbf{e} + \mathbf{K}_{m4}\mathbf{K}_{fl} \\
&\times \int \mathbf{e}\,dt) + \mathbf{K}_{m1}^{-1}(\mathbf{K}_{m2}\ddot{\mathbf{e}} + \mathbf{K}_{m3}\dot{\mathbf{e}} + \mathbf{K}_{m4}\mathbf{e})
\end{aligned}
\tag{34}
$$

By substituting (34) into (31), the error dynamics is obtained:

$$
\begin{aligned}
\mathbf{K}_{m1}\dddot{\mathbf{e}} &+ (\mathbf{K}_{m1}\mathbf{K}_{fl} + \mathbf{K}_{m2})\ddot{\mathbf{e}} + (\mathbf{K}_{m2}\mathbf{K}_{fl} + \mathbf{K}_{m3})\dot{\mathbf{e}} \\
&+ (\mathbf{K}_{m3}\mathbf{K}_{fl} + \mathbf{K}_{m4})\mathbf{e} + \mathbf{K}_{m4}\mathbf{K}_{fl} \int \mathbf{e}\,dt \quad \mathbf{0}_{3\times3} \\
&(\mathbf{K}_{m1}s^3 + \mathbf{K}_{m2}s^2 + \mathbf{K}_{m3}s + \mathbf{K}_{m4}) \\
&\times (\mathbf{I}_{3\times3}s + \mathbf{K}_{fl})\mathbf{E}(s) \quad \mathbf{0}_{3\times3}
\end{aligned}
\tag{35}
$$

With $\mathbf{K}_{fl}$ a diagonal matrix, $\mathbf{I}_{33}$ the identity matrix and $\mathbf{E}(s)$ the Laplace transform of the error vector. As observed in the Fig. 7, the dynamics are governed by complex roots related with low damped mechanical poles of the structure (resonance of the three main degrees of freedom), by fast real roots defined by the electrical dynamics of the piezoelectric actuators, and by lower real roots at 200 fixed by the compensation term $\mathbf{K}_{fl}$. The latter is the one adjusted for obtaining the desired closed loop response of the system. The detail of the root values can be found in the Table 1.

The selected controller is easy to adjust in the real platform because only the three diagonal elements in $\mathbf{K}_{fl}$ should be tuned, and each of them corresponds with a single degree of freedom. This control strategy also avoids the instability problems that are common when trying to place all the poles of the error dynamics by using state feedback in the flat representation. As observed in the Fig. 7 the mechanical poles are very low damped, and slight errors in its identification, or the presence of higher order unmodelled dynamics from the intermediate masses and the restricted degrees of freedom results in unstable behaviors.

- Hysteresis compensator: the system described in (27) does not explicitly considers the effect of hysteresis. However, piezoelectric actuators suffer from this phenomenon which affects the performance of the actuator modifying its response with respect to the input voltage. In (25) this variation is reflected in the changing value of C'. The method proposed in the present paper uses a hysteresis compensation for the variation in C' of the shape [28]:

$$
V_i \quad V_{1,i} + V_{hc,i} \quad V_{1,i} + q_i\left(\frac{1}{C'} \quad \frac{1}{C}\right)
\tag{36}
$$

With V_i the voltage applied in the compensator i, and $V_{1,i}$ the voltage applied according to the linear control strategy (30) (Fig. 6).

When included this compensation in (25), the nonlinear term q/C' is substituted by the linear one q/C.

For applying this compensator, it is necessary to online estimate the variables in (36):

The charge q_i: an estimation of the charge is obtained by using the mechanical equivalence of a piezoelectric actuator with a spring of constant k_p [24]:

Flexure	1	2	3	4	5
k_b (Nm/rad)	104.7	104.7	209.4	110.7	105.8
k_{b2} (Nm/rad)	268.4	272.7	1251.4	4603.2	113.7
k_t (Nm/rad)	5386.9	13239.9	32991.6	1277.0	472.6
k_a (N/m)	1.7e7	1.8e7	1.0e8	2.5e7	2.5e7

$$F_{1,i} \quad k_p(\delta_{p,i} \quad \delta_{1,i}) \quad k_p(a_{pzt}q_i + \delta_{1,i})$$
$$\rightarrow q_i \quad \frac{1}{k_p a_{pzt}}(\ F_{1,i} \quad k_p \delta_{1,i}) \qquad (37)$$

In (37) $F_{1,i}$ is estimated using (18). The displacement x_i is obtained from the strain gauges embedded $\delta_{1,i}$ in the actuators and the lever relationship b/a. F_i is calculated from (19) and the geometrical relationship (11). The values in acceleration and speed can be obtained from the accelererometers mounted on the platform and again from the embedded strain gauges.

The estimation of the voltage drop in the capacitor is based on (25):

$$\left(\frac{q_i}{C'}\right) \approx V_i + a_{pzt}F_{1,i} \qquad (38)$$

In this expression, the voltage at the resistance R_e is neglected, and the value $V_i(t)$ is substituted by the one from previous iteration $V_i(t \quad \delta t)$, so that the algebraic loop is avoided. This is a logical assumption, taking into account that the sample time δt is much shorter than the response time of the system.

Including (37) and (38) into (36), and using (18), (1), (10) and (19) the following expression is obtained:

$$\mathbf{v}_{hc} \quad \mathbf{v} + \mathbf{K}_{hc1}\ddot{\mathbf{x}}_{abc} + \mathbf{K}_{hc2}\dot{\mathbf{x}}_{abc} + \mathbf{K}_{hc3}\mathbf{\Delta}_1 \qquad (39)$$

where $\mathbf{v}_{hc} \in R_{3\times1}$, $\mathbf{K}_{hci} \in R_{3\times3}$ for $i = 1, 2, 3$.

$$\mathbf{K}_{hc1} \quad \left(a_{pzt} + \frac{1}{k_p Ca_{pzt}}\right)\mathbf{B}_1\mathbf{T}_f^{\ 1}\mathbf{M}\left(\mathbf{T}_f^T\right)^{\ 1}$$
$$\mathbf{K}_{hc2} \quad \left(a_{pzt} + \frac{1}{k_p Ca_{pzt}}\right)\mathbf{B}_1\mathbf{T}_f^{\ 1}\mathbf{C}_v\left(\mathbf{T}_f^T\right)^{\ 1}$$
$$\mathbf{K}_{hc3} \quad \left(a_{pzt} + \frac{1}{k_p Ca_{pzt}}\right)\left(\mathbf{B}_1\mathbf{T}_f^{\ 1}\mathbf{D}\left(\mathbf{T}_f^T\right)^{\ 1} + \mathbf{B}_2\right)\frac{b}{a} + \frac{1}{Ca_{pzt}}\mathbf{I}_{3\times3}$$
$$(40)$$

All the variables required for calculating (39) can be directly measured and therefore used for obtaining the estimated value. As the voltage has a negative gain with respect to **x**, terms $\mathbf{K}_{hc1}$, $\mathbf{K}_{hc2}$ and $\mathbf{K}_{hc3}$ behave as a acceleration, velocity and position feedback, respectively.
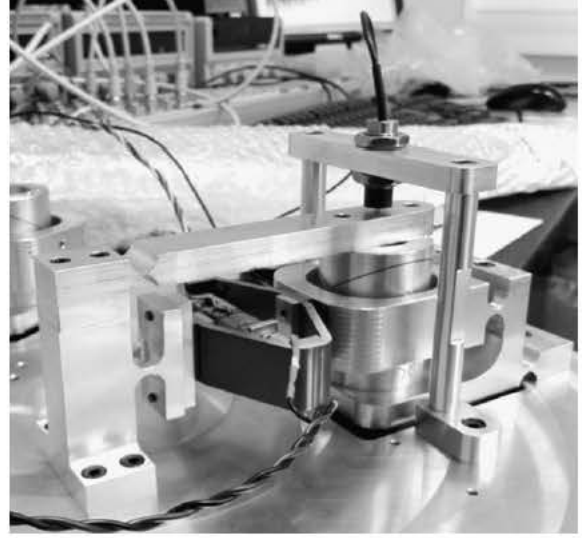

Fig. 10. Bench used for the identification of the platform.

5. Experimental results

Previous sections were focused on the design of the system from a theoretical point of view. In this section, we prove the validity of the approach by describing:

- The methodology for the sizing of the flexures.
- The methodology for the system identification.
- The validation of the control strategy.

5.1. Methodology for the sizing of the flexures

The sizing of the different flexures is arranged with two requirements:

- Resonance frequency of the platform in the principal directions of movement above 100 Hz and lower than the resonance frequency in the restricted directions of movement. This condition limits the lowest values for the stiffness of the flexures.
- The reduction in the piezoelectric stroke due to the stiffness of the system below 20%. This condition limits the highest stiffness of the flexures, because the higher it is, the higher the load in the actuator and the lower its stroke. This effect is furtherly used during the system identification.

Fig. 8 shows the way the mathematical models derived so far are used for sizing the flexures:

1. Initially, the two requirements above are converted into local stiffness of each flexure by using the derived mathematical models: the terms in (17) relate the stiffness of the flexures that
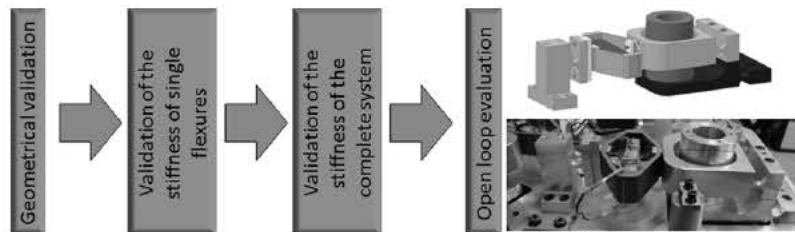

Fig. 9. Flow chart describing the validation procedure of the manufactured platform.
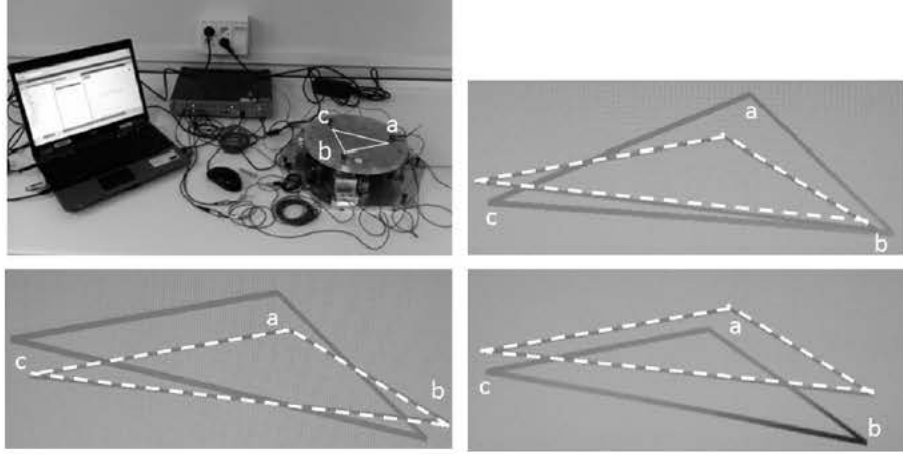
Fig. 11. Modal results obtained using OMA: first mode (top); second mode (bottom left); and third mode (bottom right). The dotted line represents the reference position.

$$\frac{b}{a} \qquad \frac{x_i}{\delta_{1,i}} \tag{41}$$

Table 3
Resonant frequencies.

Mode	OMA	Mechanical model (17)
1	186	185
2	200	202
3	214	211

affect the resonance frequency of the platform in the three main degrees of freedom (z, θ_x and θ_y); expressions (20), (22) and (24) describe the effect of the stiffness of the flexures in the restricted degrees of freedom (x, y and θ_z). Using these simpli fied mathematical expressions, the desired stiffness of the flex ures is fixed and communicated to the mechanical engineer for the flexure sizing.

2. This initial stiffness value is used for sizing the flexures (height, thickness, material). This is done using bibliographical refer ences like [19 21], and finite element models of single flexures. During this process commonly arises the necessity to update the initial stiffness obtained in the previous phase. In those cases, the simplified expressions (17), (20), (22) and (24) are used for evaluating the effect caused by the modifications.
3. Finally, the complete design is validated using FEM software. Like before, several design loops are not unusual in this phase.

The final stiffness of each flexure appears in the Table 2.

5.2. Methodology for the system identification

The control strategy described in Section 4 depends on param eters affected by geometrical and stiffness values (30). In conse quence, prior to the implementation of the controller, the manufactured platform is identified and validated in four consecu tive steps (Fig. 9), so that the results permit a fine tuning of the parameters:

1. Geometrical validation: all parts are completely measured according to the drawings. Apart from that, given its impor tance, the lever effect is also evaluated using the bench in Fig. 10. By comparing the displacement $\delta_{1,i}$ measured in the strain gauge and the displacement x_i measured by an inductive sensor, the lever relation is obtained as (1) and (6):

2. Validation of the stiffness of a single actuation line: using the bench in Fig. 10, the stiffness of one actuation line can be esti mated by comparing the displacement of the actuator before ($\delta_{p,i}$) and after ($\delta_{1,i}$) installing it in the line. This can be done, because the deformation of the actuator in presence of an exter nal spring load varies from that obtained in free conditions when the same voltage is applied. Using (8), the following rela tionship between the stiffness values is obtained:

$$k_{b,2} + k_{b,3} + k_{b,4} \qquad k_{e1}\, a^2 \left(\frac{\delta_{p,i}}{\delta_{1,i}} \right) \tag{42}$$

With this method, the most important stiffness values can be exper imentally obtained. The bending stiffness in flexure 5 is not so important given the low rotation they suffer.

3. Validation of the stiffness of the complete system: comparison of the estimated frequency responses in the theoretical model and the experimentally obtained. The obtained modes are depicted in Fig. 11: the first one corresponds with a rotation in the y axis; the second one, with a rotation in the x axis; and the third one with a displacement in z axis. For obtaining them, Operational Modal Analysis (OMA) is used. This method
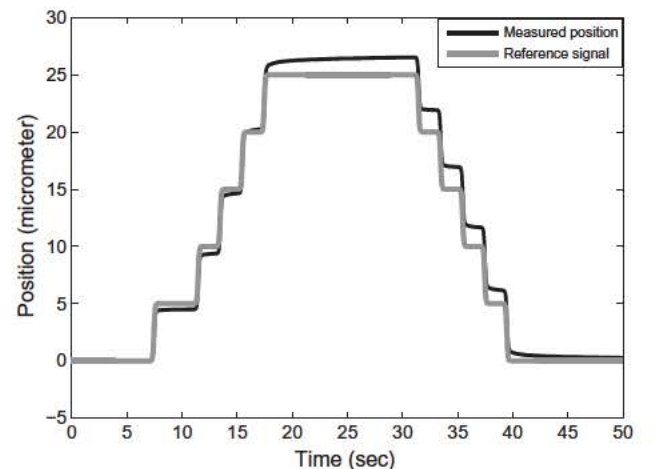

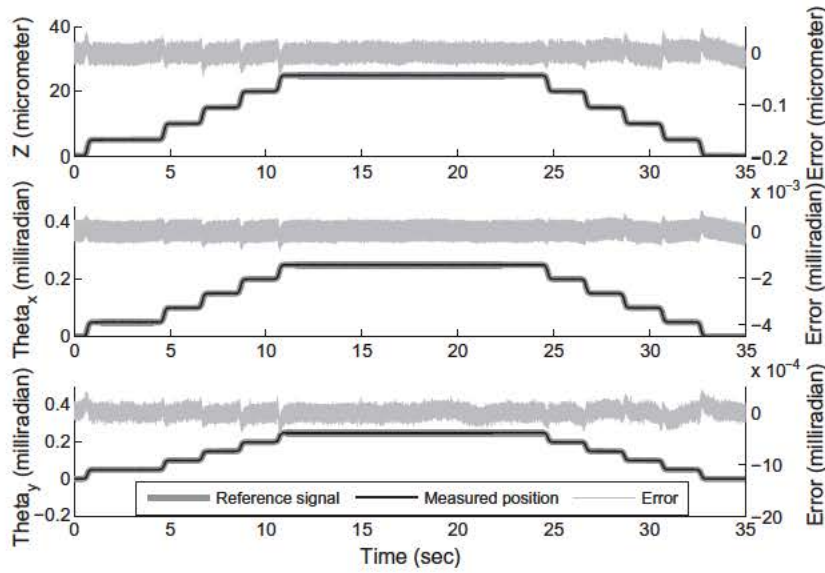Fig. 12. Open loop positioning performance of the system.

Fig. 13. Behavior of the control strategy in static positioning applications.
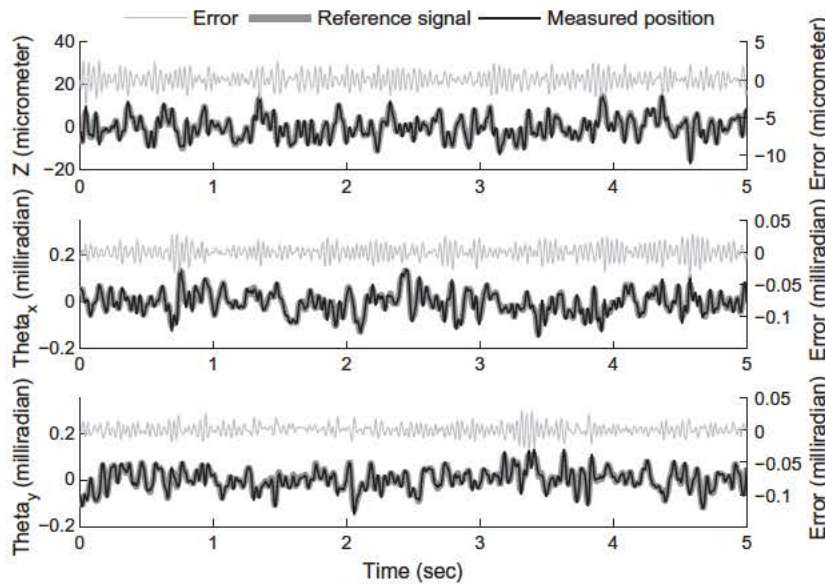

Fig. 14. Behavior of the control strategy in tracking applications without hysteresis compensation.

is a pure mechanical experiment based on exciting the structure with mechanically induced friction. The response of the system is measured using accelerometers. A summary of the obtained results are in Table 3.

For the validation of the stiffness values, the OMA test is arranged in short circuit conditions, because of the influence of the electric charge in the effective stiffness in the actuator (37) and the variation of the charge depending on the voltage at the terminals of the actuator (25).

At higher frequencies, resonances related with the intermediate elements and with the upper platform appear (restricted degrees of freedom). These effects should be taken into account in the model used for control, if higher frequency ranges were intended to be reached.

4. Open loop evaluation: the displacement predicted by the model and the experimental one are compared in an open loop test.

Fig. 12 shows the behavior of the system, if it is excited with the theoretical voltage calculated using (30). As observed, the matching is good at low displacement level in the first part of the test, but the results get poorer when displacement level increases and the direction of movement changes because of the nonlinear hysteresis phenomenon.

5.3. Positioning and tracking performance

Once the manufactured platform is identified following the previous procedure, the obtained results are used for fixing the values of the diffeomorphism parameters K_{m1}, K_{m2}, K_{m3} and K_{m4} from the control law (30). Once fixed, the compensator K_{fl} is checked in the real platform and tuned for obtaining the desired behavior.

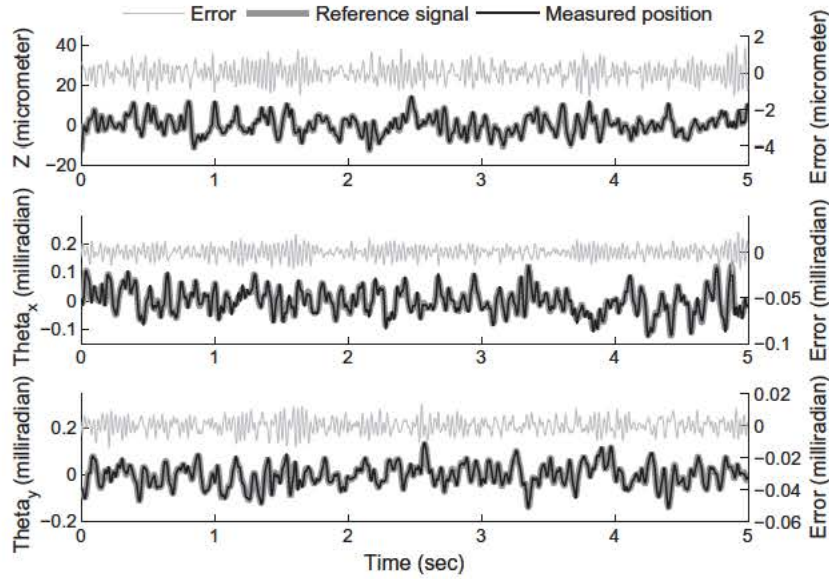The implementation of the control rests on the following elements:

Fig. 15. Behavior of the control strategy in tracking applications with hysteresis compensation.
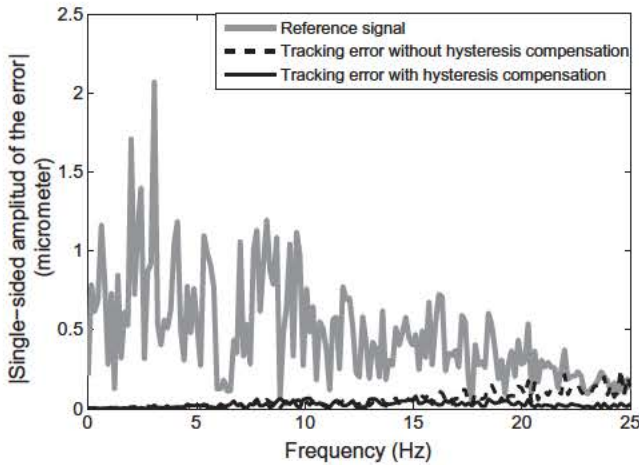

Fig. 16. Frequency comparison of the system response with and without hysteresis compensator.

- The strain gauges embedded in the actuators are used for esti mating the position of the upper platform y, and the accelerom eters are used for estimating y, and its integration ẏ. (10) permits transforming from the local measured values to the required global coordinates.
- dSpace DS1103 © control board has been used for the imple mentation of the control strategy and the sensor acquisition.

Figs. 13 15 show the behavior of the proposed control strategy and the effect of the hysteresis compensator. Two different tests have been done:

- Static positioning: a pyramid like reference signal is used for evaluating the capability of the system for positioning itself at a desired reference position (see Figs. 12 and 13). For fulfilling the continuity restriction required for the reference trajectory according to the flatness based controller, the steps are obtained by using hyperbolic functions:

$$x_{ref} \quad A_{gain}(1 + \tanh(\lambda(t \quad t_0))) \qquad (43)$$

with A_{gain}, the amplitude of the signal, λ the slope of the step, and t_0 the time shift used for starting the steps at different times.

Fig. 12 shows the limitation of using an open loop control. As ob served, the system is capable of performing steps of the required size, but the hysteresis effect and model uncertainties burden its performance. For this reason, it is necessary to include the hystere sis compensator and the closed loop controller.

Fig. 13 shows the response of the system in closed loop conditions when the reference signals are used. The system response matches the reference trajectory with errors below 18 nm in elevation, and 0.21 μ rad in rotation.

- Tracking of a random signal: the reference signals are obtained using an uniformly distributed random signal with a frequency content limited by a continuous filter. In tracking applications, the hysteresis compensator highly improves the system response. This can be observed in Figs. 14 and 15. The first one shows the system response in absence of the compensator, and the second the improvement obtained by including the hys teresis compensator. In the first case, the system cannot react at the required speed.

A more graphical description of the effect of the hysteresis com pensator appears in Fig. 16. As observed, the error increases with frequency in the absence of the compensator.

6. Conclusions

The present work shows the methodology followed for the de sign of a three axis platform. This platform is specially intended for positioning and tracking applications in combination with a metro logical device to be placed on it. With respect to previous approaches, the present work proposes a fully theoretical model of the system, which clearly shows the effect of the different elements in the behavior of the system (geometry and hinge stiffness). This model is used as a basis for sizing the flexures by relating its stiffness to the requirements of the platform in its 6 degrees of freedom.

The same model is used for designing a control strategy applying differential flatness. As the system is controllable, its states and inputs can be directly expressed in terms of the flat outputs, which in this case correspond with the trajectory to fol low. As a consequence of this property: the obtainment of the

open loop feedforward command is straightforward using the diffeomorphism between the original system and its flat representation; at the same time, the closed loop control can be designed in a decoupled way using the flat representation. Apart from that, the closed loop control used in this application depends on a single parameter, which has been of great importance during the tuning process of the controller in the real system. It is also more robust to modeling errors than the classical state feedback normally used in flat controls. The only restrictions of the proposed control are: continuity of the reference signal up to the third derivative, and frequency content of the signal in the range of validation of the model (it only contemplates the first three resonance frequencies).

The previous control design can be done using a linear approach thanks to the introduction of a hysteresis compensator. This last linearizes the behavior of the system by compensating the effect of hysteresis, which has an important impact on the system performance during fast tracking applications (20 Hz). This is the first time this compensation method is used in tracking applications (it was previously used in active vibration control systems), but after adapting it to the case under study, it has properly worked showing an important improvement in the system behavior.

Acknowledgments

Appendix A. Nomenclature

Stiffness in the different flexures.

$\mathbf{x}$	main degrees of freedom (z, θ_x, θ_y) [m, rad, rad]
$\mathbf{x}_{abc}$	displacement of the actuation lines (x_a, x_b, x_c) [m]
$x_{l,i}$	displacement of the actuation line i in the longitudinal direction (Fig. 4) [m]
$x_{t,i}$	displacement of the actuation line i in the transversal direction (Fig. 4) [m]
$\alpha_{j,i}$	angle of the joint j in its preferred direction in the actuation line i (dotted lines in Fig. 2) [rad]
$\alpha_{tj,i}$	torsion angle of the joint j in the actuation line i [rad]
$\alpha_{b2,j,i}$	angle of the joint j in the third rotation direction in the actuation line i [rad]
$\delta_{j,i}$	deformation of the segment L_j in actuation line i [m]
$\boldsymbol{\Delta}_{abc}$	displacement of a piezoelectric actuator without external loads in the three actuation lines $(\delta_{p,a}, \delta_{p,b}, \delta_{p,c})$ [m, m, m]
$\boldsymbol{\Delta}_1$	deformation of the horizontal beam in the three actuation lines $(\delta_{1,a}, \delta_{1,b}, \delta_{1,c})$ [m, m, m]
$\mathbf{f}_{ext}$	external forces and torques affecting the upper platform $(F_{z,ext}, \Gamma_{x,ext}, \Gamma_{y,ext})$ [N, Nm, Nm]
$\mathbf{f}$	forces affecting the actuation lines because of the upper platform $(F_z, \Gamma_x, \Gamma_y)$ [N, Nm, Nm]
$\mathbf{f}_{abc}$	forces at the top of the actuation lines (F_a, F_b, F_c) [N, N, N]
$F_{1,i}$	force in segment 1 of the actuation line i [N]
$F_{l,i}$	force of the actuation line i in the longitudinal direction (Fig. 4) [N]

$F_{t,i}$	force of the actuation line i in the transversal direction (Fig. 4) [N]
L_i	length of the bar i [m]
$L_{1,j}$	length of the bar 1 in section j (1: from $P1$ to $Pp1$; 2: from $Pp1$ to $Pp2$; 3: from $Pp2$ to $P2$) (Fig. 2) [m]
r	distance from the center of the platform to the actuation points a, b and c [m]
$\mathbf{T}_f$	transformation matrix between the local and global coordinates $\begin{pmatrix} 1 & 1 & 1 \\ 0 & r\cos(\pi/6) & r\cos(\pi/6) \\ r & r\sin(\pi/6) & r\sin(\pi/6) \end{pmatrix}$
$k_{a,i}$	axial stiffness of the flexure i [N/m]
$k_{b,i}$	rotation stiffness of the flexure i in the direction described in Fig. 3 [Nm/rad]
$k_{t,i}$	torsional stiffness of the flexure i [Nm/rad]
$k_{b2,i}$	rotation stiffness of the flexure i in the third rotation direction [Nm/rad]
k_p	axial stiffness of the piezoelectric actuator [N/m]
k_x	stiffness of the platform in the restricted degree of freedom x [N/m]
k_y	stiffness of the platform in the restricted degree of freedom y [N/m]
k_{bz}	torsion stiffness of the platform x [Nm/rad]
k_l^{al}	stiffness of an actuation line in the permitted direction [Nm/m]
k_t^{al}	stiffness of an actuation line in the restricted direction [Nm/m]
$k_{5,xy}$	coupled stiffness between longitudinal and transversal direction in the flexure 5 [Nm/rad]
$\mathbf{k}_{b5}$	stiffness matrix $\begin{pmatrix} k_{b,5} & k_{5,xy} \\ k_{5,xy} & k_{b2,5} \end{pmatrix}$
$\mathbf{K}_{\alpha 5}$	stiffness matrix $\begin{pmatrix} \mathbf{k}_{b5} & \mathbf{0} & \mathbf{0} \\ \mathbf{0} & \mathbf{k}_{b5} & \mathbf{0} \\ \mathbf{0} & \mathbf{0} & \mathbf{k}_{b5} \end{pmatrix}$
$\mathbf{T}_{\alpha 5}$	transformation matrix $\begin{pmatrix} \cos(\pi/3) & \cos(\pi/6) \\ \sin(\pi/3) & \sin(\pi/6) \\ \cos(\pi/3) & \cos(\pi/6) \\ \sin(\pi/3) & \sin(\pi/6) \\ 1 & 0 \\ 0 & 1 \end{pmatrix}$
$\mathbf{M}$	inertia matrix of the platform [kg, kg m^2, kg m^2] $\begin{pmatrix} M & 0 & 0 \\ 0 & J_x & 0 \\ 0 & 0 & J_y \end{pmatrix}$
$\mathbf{D}$	stiffness matrix related with the angular movement of the platform $\begin{pmatrix} 0 & \mathbf{0}_{1\times 2} \\ \mathbf{0}_{2\times 1} & \mathbf{T}_{\alpha 5}^T \mathbf{K}_{\alpha 5} \mathbf{T}_{\alpha 5} \end{pmatrix}$
$\mathbf{C}_v$	viscous friction coefficient matrix associated with the actuation lines
a_{pzt}	electromechanical transformation factor of the piezoelectric actuator [m/C]
$\mathbf{v}$	voltage applied V_i for $i = a$, b, c [V]
$\mathbf{v}_1$	flatness based control command $V_{1,i}$ for $i = a$, b, c [V]
$\mathbf{v}_{hc}$	hysteresis compensation voltage $V_{hc,i}$ for $i = a$, b, c [V]
$\mathbf{v}_{1,ff}$	feedforward term in the flatness based control [V]
$\mathbf{v}_{1,fb}$	feedback term in the flatness based control [V]
q_i	charge in the piezoelectric capacitor i [C]
R_e	electric resistance from amplifier to actuator [Ω]
C'	capacitance of the actuator [Ω]
C	mean value of the capacitance of the actuator [Ω]

The geometrical parameters $(t_4, \beta, t_2, a, b, L_1, L_2)$ appear in Figs. 2 and 3.

Appendix B. Coefficients of the electromechanical model

The terms of the electromechanical model are listed below:

$$\mathbf{H}_0 \quad \mathbf{a}_{pzt}\mathbf{B}_1\mathbf{T}_f^{-1}$$

$$\mathbf{H}_1 \quad \left(\mathbf{A}_2\mathbf{T}_f^{-1}\mathbf{M}\right)^{-1}\left(\mathbf{T}_f^T + \mathbf{A}_2\mathbf{T}_f^{-1}\mathbf{D}\right)$$

$$\mathbf{H}_2 \quad \left(\mathbf{A}_2\mathbf{T}_f^{-1}\mathbf{M}\right)^{-1}\mathbf{A}_2\mathbf{T}_f^{-1}\mathbf{C}_v$$

$$\mathbf{H}_3 \quad \left(\mathbf{A}_2\mathbf{T}_f^{-1}\mathbf{M}\right)^{-1}\mathbf{A}_1\mathbf{a}_{pzt}$$

$$\mathbf{H}_4 \quad \mathbf{R}_e^{-1}(\mathbf{a}_{pzt}\mathbf{B}_2\mathbf{T}_f^T + \mathbf{H}_0\mathbf{D} \quad \mathbf{H}_0\mathbf{M}\mathbf{H}_1) \qquad (B.1)$$

$$\mathbf{H}_5 \quad \mathbf{R}_e^{-1}(\quad \mathbf{H}_0\mathbf{M}\mathbf{H}_2 + \mathbf{H}_0\mathbf{C}_v)$$

$$\mathbf{H}_6 \quad \mathbf{R}_e^{-1}(\quad \mathbf{C}^{-1} \quad \mathbf{H}_0\mathbf{M}\mathbf{H}_3)$$

$$\mathbf{H}_7 \quad \mathbf{R}_e^{-1}$$

where

k_{e1}	equivalent axial stiffness of the beam (Fig. 2): $\left(\frac{1}{k_{a,1}} + \frac{1}{k_{a,2}} + \frac{1}{k_p}\right)^{-1}$
k_{e3}	equivalent axial stiffness of the pillar (Fig. 2): $\left(\frac{1}{k_{a,4}} + \frac{1}{k_{a,5}}\right)^{-1}$
A_1	variation gain of x_i because of $\delta_{p,i}$ [ ] $\frac{k_{e1}ab}{k_{e1}a^2+(k_{b,2}+k_{b,3}+k_{b,4})}$
A_2	variation gain of x_i because of F_i [m/N] $\left(\frac{1}{k_{e3}} + \frac{ab^2}{k_{e1}a^3+(k_{b,2}+k_{b,3}+k_{b,4})}\right)$
B_1	variation gain of F_i because of F [ ] $\frac{b}{a} + \frac{1}{bk_{e3}a}(k_{b,2}+k_{b,3}+k_{b,4})$
B_2	variation gain of F_i because of x [N/m] $\frac{1}{ba}(k_{b,2}+k_{b,3}+k_{b,4})$

$\mathbf{A}_1$, $\mathbf{A}_2$, $\mathbf{B}_1$, $\mathbf{B}_2$, $\mathbf{R}_e$, $\mathbf{C}$ and $\mathbf{a}_{pzt}$ are diagonal matrices with the terms in the diagonal equal to the scalar value of the same name.

Appendix C. Coefficients of k_t^{al}

The terms of (24) are defined below (for clarity reason, subindex i for the actuation line is eliminated):

$$G_0 = \frac{k_{t,p1}k_{t,p2}k_{t,2}a}{k_{t,p1}k_{t,p2}k_{t,2} + k_{t,1}k_{t,p2}k_{t,2} + k_{t,1}k_{t,p1}k_{t,2} + k_{t,1}k_{t,p1}k_{t,p2}}$$

$$G_1 = \frac{L_1^2}{k_{b2,1}} + \frac{(L_{1,2}+L_{1,3})^2}{k_{b2,p1}} + \frac{L_{1,3}^2}{k_{b2,p2}}$$

$$G_2 = \frac{L_1}{k_{b2,1}} + \frac{L_{1,2}+L_{1,3}}{k_{b2,p1}} + \frac{L_{1,3}}{k_{b2,p2}}$$

$$G_3 = \frac{1}{k_{b2,1}} + \frac{1}{k_{b2,p1}} + \frac{1}{k_{b2,p2}} + + \frac{1}{k_{b2,2}}$$

$$G_4 = \frac{1}{G_2 a}\left(G_2 a + \frac{L_3}{b}(k_{b2,3} \quad 0.5k_{t,4})\left(G_2^2 \quad G_1 G_3\right)\right)$$

$$G_5 = \frac{1}{G_2 ab}(k_{b2,3} \quad 0.5k_{t,4})\left(\quad G_2^2 + G_1 G_3\right)$$

$$G_6 = \frac{b}{G_2 a}\left(G_2^2 \quad G_1 G_3\right)$$

$$G_7 = \frac{\frac{aG_2}{bG_1}(k_{b2,3} \quad 0.5k_{t,4}) + G_5\left(k_{b2,4}+k_{t,3}+k_{t,1}G_0 + \frac{a^2}{G_1}\right)}{G_4\left(k_{b2,4}+k_{t,3}+k_{t,1}G_0 + \frac{a^2}{G_1}\right) \quad \frac{G_2 a}{G_1 b}(k_{b2,3} \quad 0.5k_{t,4})L_3 \quad k_{t,3} \quad k_{t,1}G_0 \quad \frac{a^2}{G_1}}$$

$$G_8 = \frac{\frac{baG_2}{G_1} + a \quad G_6\left(k_{b2,4}+k_{t,3}+k_{t,1}G_0 + \frac{a^2}{G_1}\right)}{G_4\left(k_{b2,4}+k_{t,3}+k_{t,1}G_0 + \frac{a^2}{G_1}\right) \quad \frac{G_2 a}{G_1 b}(k_{b2,3} \quad 0.5k_{t,4})L_3 \quad k_{t,3} \quad k_{t,1}G_0 \quad \frac{a^2}{G_1}}$$

$$(C.1)$$

References

[1] Fliess M, Levine J, Martin Ph, Rouchon P. Sur les systèmes non linêaires différentiellement plats. Comptes Rendus de l'Académie des Sciences Paris 1992;I315:619–24.

[2] Fliess M, Levine J, Martin Ph, Rouchon P. Flatness and defect of nonlinear systems: introductory theory and examples. Int J Control 1995;61(6):1327–61.

[3] Levine J. Analysis and control of nonlinear systems: a flatness-based approach. Springer; 2009.

[4] Chen Y, McInroy JE. Decoupled control of flexure-jointed hexapods using estimated joint-space mass–inertia matrix. IEEE Trans Control Syst Technol 2004;12(3):413–21.

[5] Lee SQ, Kim Y, Gweon D-G. Continuous gain scheduling control for a micro-positioning system: simple, robust and no overshoot response. Control Eng Practice 2000;8:133–8.

[6] Vagia M, Nikolakopoulos G, Tzes A. Design of a robust PID-control switching scheme for an electrostatic microactuator. Control Eng Practice 2008;16:1321–8.

[7] Shieh H-J, Lin F-J, Huang P-K, Teng L-T. Adaptive tracking control solely using displacement feedback for a piezo-positioning mechanism. IEE Proc Control Theory Appl 2004;151(5):653–60.

[8] Liaw HC, Shirinzadeh B. Robust generalised impedance control of piezo-actuated flexure-based 4-bar mechanisms for micro/nano-manipulation. Sensors Actuat A 2008;148:443–53.

[9] Rodriguez-Fortun JM, Orus J, Alfonso J, Rotella F, JA. Castellanos, Control of a multi-axis platform for metrological purposes using differential flatness. In: 50th IEEE conference on decision and control and european control conference; 2011.

[10] Yong YK, Lu T-F. Kinetostatic modeling of 3-RRR compliant micro-motion stages with flexure hinges. Mech Mach Theory 2009;44:1156–75.

[11] Tian Y, Shirinzadeh B, Zhang D. A flexure-based mechanism and control methodology for ultra-precision turning operation. Prec Eng 2009;33:160–6.

[12] Tian Y, Shirinzadeh B, Zhang D, Alici G. Development and dynamic modelling of a flexure-based ScottRussell mechanism for nano-manipulation. Mech Syst Signal Proces 2009;23:957–78.

[13] Kim HS, Cho YM. Design and modeling of a novel 3-DOF precision micro-stage. Mechatronics 2009;19(5):598–608.

[14] Mukhopadhyay D, Dong J, Pengwang E, Ferreira P. A SOI-MEMS-based 3-DOF planar parallel-kinematics nanopositioning stage. Sensors Actuat A 2008;147:340–51.

[15] Choi Y-J, Sreenivasan SV, Choi BJ. Kinematic design of large displacement precision XY positioning stage by using cross strip flexure joints and over-constrained mechanism. Mech Mach Theory 2008;43:724–37.

[16] McInroy JE. Modeling and design of flexure jointed stewart platforms for control purposes. IEEE/ASME Trans Mech 2002;7(1):95–9.

[17] Ouyang PR, Tjiptoprodjo RC, Zhang WJ, Yang GS. Micro-motion devices technology: the state of arts review. Int J Adv Manuf Technol 2007;35(5–6):463–78.

[18] Zubir MNM, Shirinzadeh B. Development of a high precision flexure-based microgripper. Prec Eng 2009;33(4):362–70.

[19] Smith ST. Flexures: elements of elastic mechanisms. Gordon & Breach Science Publication; 2000.

[20] Lobontiu N. Compliant mechanisms: design of flexure hinges. CRC Press; 2003.

[21] Howell LL. Compliant mechanisms. John Wiley & Sons Inc.; 2001.

[22] Lobontiu N, Paine JSN, Garcia E, Goldfarb M. Design of symmetric conic-section flexure hinges based on closed-form compliance equations. Mech Mach Theory 2002;37:477–98.

[23] Zelenika S, Munteanu MGh, De Bona F. Optimized flexural hinge shapes for microsystems and high-precision applications. Mech Mach Theory 2009;44(10):1826–39.

[24] Rodriguez-Fortun JM, Orus J, Buil F, Castellanos JA. General Bond Graph model for piezoelectric actuators and methodology for experimental identification. Mechatronics 2010;20(2):303–14.

[25] Oates WS, Smith RC. Nonlinear optimal control techniques for vibration attenuation using magnetostrictive actuators. J Intell Mater Syst Struct 2008;19(2):193–209.

[26] Hwang CL, Jan C, Chen Y-H. Piezomechanics using intelligent variable-structure control. IEEE Trans Ind Electron 2001;48(1):47–59.

[27] Lin J, Lewis FL. Two-time scale fuzzy logic controller of flexible link robot arm. Fuzzy Sets Syst 2003;139(1):125–49.

[28] Rodriguez-Fortun JM, Orus J, Alfonso J, Castellanos. Nonlinear active vibration control for piezoelectric actuators. In: Proceedings of the American control conference (ACC); 2010. p. 744–749.

[29] Devasia S, Eleftheriou E, Moheimani SOR. A survey of control issues in nanopositioning. IEEE Trans Control Syst Technol 2007;15(5):802–23.

[30] Leang KK, Devasia S. Feedback-linearized inverse feedforward for creep, hysteresis, and vibration compensation in AFM piezoactuators. IEEE Trans Control Syst Technol 2007;15(5):927–35.

[31] Sebastian A, Salapaka SM. Design methodologies for robust nano-positioning. IEEE Trans Control Syst Technol 2005;13(6):868–76.